A Simple Finite-Volume Method on a Cartesian Mesh for Pedestrian Flows with Obstacles

Yuanzhen Cheng, Alina Chertock and Alexander Kurganov

Abstract We consider a two-dimensional pedestrian flow model with obstacles governed by scalar hyperbolic conservation laws, in which the flux is implicitly dependent on the density through the Eikonal equation. We propose a simple second-order finite-volume method, which is applicable to the case of obstacles of arbitrary shapes. Though the method is only first-order accurate near the obstacles, it is robust and provides sharp resolution of discontinuities as illustrated in a number of numerical experiments.

Keywords Pedestrian flow model · Hyperbolic conservation laws · Finite-volume method · Interface tracking method · Eikonal equation · Fast sweeping method

MSC (2010) 90B20 · 35L65 · 35F21 · 65M08 · 65M99

1 Introduction

In this paper, we study a two-dimensional (2-D) pedestrian flow model governed by the scalar hyperbolic conservation laws

$$\rho_t + f(\rho, \phi_x)_x + g(\rho, \phi_y)_y = 0, \tag{1}$$

Y. Cheng · A. Kurganov (✉)
Mathematics Department, Tulane University, New Orleans, LA 70118, USA
e-mail: kurganov@math.tulane.edu

Y. Cheng
e-mail: ycheng5@tulane.edu

A. Chertock
Department of Mathematics, North Carolina State University, Raleigh, NC 27695, USA
e-mail: chertock@math.ncsu.edu

A. Kurganov
Department of Mathematics, Southern University of Science and Technology of China, Shenzhen 518055, China

C. Cancès and P. Omnes (eds.), *Finite Volumes for Complex Applications VIII—Methods and Theoretical Aspects*, Springer Proceedings in Mathematics & Statistics 199, DOI 10.1007/978-3-319-57397-7_4

where ρ is the pedestrian density and $(f, g)^T$ is the flux given by

$$(f, g)^T = -\rho u \frac{\nabla \phi}{||\nabla \phi||}. \tag{2}$$

Here, ϕ is the cost potential function satisfying the Eikonal equation

$$||\nabla \phi|| = \frac{1}{u}, \tag{3}$$

and u is the isotropic walking speed

$$u := u_{\max} \left(1 - \frac{\rho}{\rho_{\max}}\right) \tag{4}$$

with $u_{\max}$ and $\rho_{\max}$ being the free-flow speed and the jam density, respectively.

This pedestrian flow model was introduced in [8] (see also [7]) as a tool to design walking facility. Note that the flux (2) is implicitly dependent on the density through the Eikonal equations (3), (4), which is a special steady-state Hamilton-Jacobi equation. It was shown in [7] that the pedestrian route choice strategy satisfies the reactive user equilibrium principle in which a pedestrian choose a route to minimize the instantaneous travel cost to the destination.

According to [7, 16], the model (1)–(4) can be used to study pedestrian flows in the domain with obstacles. In this case, the obstacles are represented by setting $\rho = 0$ and $\phi = \phi_{\max}$ inside them with $\phi_{\max}$ being a very large fixed positive number. The presence of obstacles makes the development of numerical methods for (1)–(4) a challenging task. In [7], a fifth-order finite-difference WENO scheme was developed for the simplest case of a square-shaped obstacle with the boundary aligned with a Cartesian. Obstacles, however, may be of an arbitrary shape and one may prefer to use an unstructured mesh, which can be adjusted to the shape of the obstacle, but then the implementation of the numerical method becomes much more complicated. For example, a circular obstacle was considered in [16], where a discontinuous Galerkin (DG) method on unstructured triangular mesh for (1)–(4) was introduced.

The main goal of this paper is to develop a simple second-order finite-volume method on uniform Cartesian grids, which is applicable to the case of obstacles of arbitrary shape. Here we follow the idea of the interface tracking method, which was originally developed for compressible multifluids in [3] and then extended to compressible fluids in domains with moving solid boundaries/obstacles in [4]. To this end, we cover the computational domain with a Cartesian mesh and categorize the Cartesian cells into the following three types: interior, mixed and obstacle ones. The interior cells are the ones that can be fully occupied by pedestrians. The obstacle cells are the ones that are filled by obstacles and are not accessible by pedestrians. Finally, the mixed cells are those where the obstacle boundary is located and thus only part of these cells is accessible. We update the solution in time in the interior

cells only, while the mixed cell data required for numerical flux function evaluation are obtained using an interpolation procedure.

In the interior cells, the solution is evolved using the second-order semi-discrete central-upwind (CU) scheme, which was developed in [9–12] for general multi-dimensional systems of conservation laws. The CU scheme, however, cannot be directly applied to Eq. (1), since the flux (2) depends on the derivatives of the cost potential function ϕ. To overcome this difficulty, we take advantage of the fact that CU schemes are not based on (approximate) Riemann problem solvers and the only upwinding information required is the estimate of one-sided local speeds of propagation. An additional source of difficulty comes from the fact that the flux (2) is implicitly dependent on the density ρ through the Eikonal equations (3), (4), which should be numerically solved at every time level by an efficient algorithm. We use the fast sweeping method from [17], which was designed to solve a nonlinear discretized system directly and efficiently by exploiting the causality of the Eikonal equation. We apply the fast sweeping method to evolve the cost potential in the interior and mixed cells, while keeping its values large in obstacle cells. The resulting finite-volume method is described in Sect. 2.

Compared to alternative numerical methods such as those in [7, 16], our new method is simpler yet still accurate and efficient and can be applied to general cases with obstacles of any shape as confirmed by our numerical experiments reported in Sect. 3. A potential drawback of the proposed approach is the lack of conservation as we do not evolve the pedestrian density in the mixed cells. We expect however the conservation error to be proportional to the spatial grid size similar to the conservation error in the interface tracking method reported in [4].

2 Numerical Method

In this section, we describe the numerical method for the pedestrian flow model (1)–(4).

For simplicity, we consider a rectangular computational domain covered by a uniform spatial mesh consisting of the cells $C_{j,k}$ centered at $(x_j, y_k) := (j\Delta x, k\Delta y)$. The cell is categorized as an *interior cell* if all of its four vertices, $(x_{j\pm\frac{1}{2}}, y_{k\pm\frac{1}{2}})$, are located outside the obstacles; the cell is categorized as an *obstacle cell* if all of its four vertices are located inside the obstacle; otherwise, the cell is categorized as a *mixed cell*. We introduce an indicator $I_{j,k}$, which is equal to 1 at the interior cells, 0 at the mixed cells, and -1 at the obstacle cells.

The cell averages of ρ, denoted by

$$\overline{\rho}_{j,k}(t) := \frac{1}{\Delta x\,\Delta y}\iint\limits_{C_{j,k}} \rho(x, y, t)\,dy\,dx, \quad C_{j,k} := [x_{j-\frac{1}{2}}, x_{J+\frac{1}{2}}] \times [y_{k-\frac{1}{2}}, y_{k+\frac{1}{2}}]$$

are evolved in time in the interior cells ($I_{j,k} = 1$) according to the semi-discrete scheme:

$$\frac{d}{dt}\,\overline{\rho}_{j,k}(t) = -\frac{H^x_{J+\frac{1}{2},k}(t) - H^x_{j-\frac{1}{2},k}(t)}{\Delta x} - \frac{H^y_{j,k+\frac{1}{2}}(t) - H^y_{j,k-\frac{1}{2}}(t)}{\Delta y}, \tag{5}$$

where $H^x_{j\pm\frac{1}{2},k}$ and $H^y_{j,k\pm\frac{1}{2}}$ are the numerical fluxes, whose computation depends on the type of neighboring cells. Namely, if $I_{j+1,k} = -1$ or $I_{j+1,k} = 0$ and $I_{j+2,k} = -1$, then we set $H^x_{J+\frac{1}{2},k} = 0$ since the pedestrians will not walk directly into the obstacle. In other cases, we use the second-order CU flux from [10]:

$$H^x_{J+\frac{1}{2},k} := \frac{a^+_{J+\frac{1}{2},k} f^{\mathrm{E}}_{j,k} - a^-_{J+\frac{1}{2},k} f^{\mathrm{W}}_{j+1,k}}{a^+_{J+\frac{1}{2},k} - a^-_{J+\frac{1}{2},k}} + \frac{a^+_{J+\frac{1}{2},k} a^-_{J+\frac{1}{2},k}}{a^+_{J+\frac{1}{2},k} - a^-_{J+\frac{1}{2},k}} \left[\rho^{\mathrm{W}}_{j+1,k} - \rho^{\mathrm{E}}_{j,k}\right]. \tag{6}$$

The y-fluxes are obtained in a similar way, that is, if $I_{j,k+1} = -1$ or $I_{j,k+1} = 0$ and $I_{j,k+2} = -1$, then we set $H^y_{j,k+\frac{1}{2}} = 0$, while the second-order CU flux from [10],

$$H^y_{j,k+\frac{1}{2}} := \frac{b^+_{j,k+\frac{1}{2}} g^{\mathrm{N}}_{j,k} - b^-_{j,k+\frac{1}{2}} g^{\mathrm{S}}_{j,k+1}}{b^+_{j,k+\frac{1}{2}} - b^-_{j,k+\frac{1}{2}}} + \frac{b^+_{j,k+\frac{1}{2}} b^-_{j,k+\frac{1}{2}}}{b^+_{j,k+\frac{1}{2}} - b^-_{j,k+\frac{1}{2}}} \left[\rho^{\mathrm{S}}_{j,k+1} - \rho^{\mathrm{N}}_{j,k}\right], \tag{7}$$

are used in other cases. In (6) and (7), we use the following notation

$$\begin{aligned} f^{\mathrm{E}}_{j,k} &:= f(\rho^{\mathrm{E}}_{j,k}, (\phi_x)_{J+\frac{1}{2},k}), \quad f^{\mathrm{W}}_{j+1,k} := f(\rho^{\mathrm{W}}_{j+1,k}, (\phi_x)_{J+\frac{1}{2},k}), \\ g^{\mathrm{N}}_{j,k} &:= g(\rho^{\mathrm{N}}_{j,k}, (\phi_y)_{j,k+\frac{1}{2}}), \quad g^{\mathrm{S}}_{j,k+1} := g(\rho^{\mathrm{S}}_{j,k+1}, (\phi_y)_{j,k+\frac{1}{2}}), \end{aligned} \tag{8}$$

where $\rho^{\mathrm{E}}_{j,k}$, $\rho^{\mathrm{W}}_{j+1,k}$, $\rho^{\mathrm{N}}_{j,k}$ and $\rho^{\mathrm{S}}_{j,k+1}$ are reconstructed cell interface density values (see Sect. 2.1 for details), $(\phi_x)_{J+\frac{1}{2},k}$ and $(\phi_y)_{j,k+\frac{1}{2}}$ are numerical derivatives of ϕ obtained from the solution of the Eikonal equations (3), (4) as discussed in Sect. 2.2 below, and $a^{\pm}_{J+\frac{1}{2},k}$ and $b^{\pm}_{j,k+\frac{1}{2}}$ are estimated one-sided local speeds of propagation defined in Sect. 2.3. We note that all of the above indexed quantities (except for $I_{j,k}$) depend on t, but we omit this dependence for the sake of brevity.

Remark 1 The semi-discretization (5) is a system of time-dependent ODEs, which should be solved by a stable and sufficiently accurate ODE solver. In all of our numerical experiments, we have used the three-stage third-order strong stability preserving Runge–Kutta (SSP-RK) method (see, e.g., [5, 6]) with the CFL number 0.25.

Remark 2 Positivity of the evolved values of $\overline{\rho}_{j,k}$ is enforced using the draining time step technique, which was proposed in the context of the one-dimensional shallow water equations in [1] and then extended to a general 2-D finite-volume evolution in [2].

2.1 Evaluation of Point Values of ρ

The reconstruction of point values of the pedestrian cell density depends on the type of the cell these quantities are computed in.

Interior cells. We approximate the pedestrian density in these cells using a piecewise linear interpolant

$$\widetilde{\rho}(x, y) = \overline{\rho}_{j,k} + (\rho_x)_{j,k}(x - x_j) + (\rho_y)_{j,k}(y - y_k),$$

which is second-order accurate and non-oscillatory provided the slopes $(\rho_x)_{j,k}$ and $(\rho_y)_{j,k}$ are computed using a nonlinear limiter. The slopes are evaluated as follows (we will only discuss the computation of $(\rho_x)_{j,k}$ since $(\rho_y)_{j,k}$ are obtained in a similar way).

If both $I_{j\pm1,k} = 1$, then $(\rho_x)_{j,k}$ are computed using the generalized minmod limiter (see, e.g., [13–15]):

$$(\rho_x)_{j,k} = \text{minmod}\left(\theta\,\frac{\overline{\rho}_{j,k} - \overline{\rho}_{j-1,k}}{\Delta x},\ \frac{\overline{\rho}_{j+1,k} - \overline{\rho}_{j-1,k}}{2\Delta x},\ \theta\,\frac{\overline{\rho}_{j+1,k} - \overline{\rho}_{j,k}}{\Delta x}\right),$$

where the minmod function is defined as

$$\text{minmod}(z_1, z_2, \ldots) := \begin{cases} \min_j\{z_j\}, & \text{if } z_j > 0,\ \forall j, \\ \max_j\{z_j\}, & \text{if } z_j < 0,\ \forall j, \\ 0, & \text{otherwise,} \end{cases}$$

and $\theta \in [1, 2]$ is a parameter that can be used to control the amount of numerical viscosity present in the resulting scheme. In all of our numerical experiments, we have taken $\theta = 1.3$.

In the interior cells located near the obstacle, that is if either $I_{j+1,k} \neq 1$ or $I_{j-1,k} \neq 1$, we set $(\rho_x)_{j,k} = 0$.

The point values at the centers of cell interfaces required in (6)–(8) are then obtained using $\widetilde{\rho}$:

$$\rho^{\text{E}}_{j,k} = \widetilde{\rho}(x_{J+\frac{1}{2}}, y_k),\ \ \rho^{\text{W}}_{j,k} = \widetilde{\rho}(x_{j-\frac{1}{2}}, y_k),\ \ \rho^{\text{N}}_{j,k} = \widetilde{\rho}(x_j, y_{k+\frac{1}{2}}),\ \ \rho^{\text{S}}_{j,k} = \widetilde{\rho}(x_j, y_{k-\frac{1}{2}}).$$

Similarly, one can compute the point values at the corners of the cell $C_{j,k}$:

$$\begin{aligned} \rho^{\text{NE}}_{j,k} &= \widetilde{\rho}(x_{J+\frac{1}{2}}, y_{k+\frac{1}{2}}), & \rho^{\text{NW}}_{j,k} &= \widetilde{\rho}(x_{j-\frac{1}{2}}, y_{k+\frac{1}{2}}), \\ \rho^{\text{SE}}_{j,k} &= \widetilde{\rho}(x_{J+\frac{1}{2}}, y_{k-\frac{1}{2}}), & \rho^{\text{SW}}_{j,k} &= \widetilde{\rho}(x_{j-\frac{1}{2}}, y_{k-\frac{1}{2}}), \end{aligned}$$

which will be needed only in some interior cells located near the obstacle; see below.

Mixed cells. In these cells, we first compute the values of $\overline{\rho}_{j,k}$, which are obtained from the nearby interior cells using the interpolation technique introduced in [3, Sect. 2.3.1] and set the corner values in the mixed cells to be

$$\rho^{\mathrm{NE}}_{j,k} = \rho^{\mathrm{NW}}_{j,k} = \rho^{\mathrm{SE}}_{j,k} = \rho^{\mathrm{SW}}_{j,k} = \overline{\rho}_{j,k}.$$

We then obtain the point values of ρ at the centers of cell interfaces by the following interpolating procedure:

$$\rho^{\mathrm{E}}_{j,k} = \frac{1}{2}\left(\rho_{J+\frac{1}{2},k+\frac{1}{2}} + \rho_{J+\frac{1}{2},k-\frac{1}{2}}\right),$$

where

$$\rho_{J+\frac{1}{2},k+\frac{1}{2}} := \frac{1}{4}\left(\frac{I_{j,k}+1}{2}\rho^{\mathrm{NE}}_{j,k} + \frac{I_{j,k+1}+1}{2}\rho^{\mathrm{SE}}_{j,k+1} + \frac{I_{j+1,k+1}+1}{2}\rho^{\mathrm{SW}}_{j+1,k+1} + \frac{I_{j+1,k}+1}{2}\rho^{\mathrm{NW}}_{j+1,k}\right).$$

Here, the use of factors $(I_{\ell,m}+1)/2$ leads to reducing the contribution of the values from the mixed cells (in which $I_{\ell,m} = 0$) by a factor of 2 since it is reasonable to assume that in the case of general shape obstacles, only half (in average) of the mixed cells are occupied by the pedestrians. The point values $\rho^{\mathrm{W}}_{j,k}$, $\rho^{\mathrm{N}}_{j,k}$ and $\rho^{\mathrm{S}}_{j,k}$ are obtained similarly.

Remark 3 We note that the order of the CU scheme near the obstacles reduces to the first one as in the interface tracking method from [3, 4]. However, we still use second-order CU scheme away from the obstacles since this is necessary to achieve a sharp resolution of the shock waves.

2.2 Computation of ϕ_x and ϕ_y

The values of $(\phi_x)_{J+\frac{1}{2},k}$ and $(\phi_y)_{j,k+\frac{1}{2}}$ needed in (8) are computed using the centered differences:

$$(\phi_x)_{J+\frac{1}{2},k} = \frac{\phi_{j+1,k} - \phi_{j,k}}{\Delta x} \quad \text{and} \quad (\phi_y)_{j,k+\frac{1}{2}} = \frac{\phi_{j,k+1} - \phi_{j,k}}{\Delta y}, \tag{9}$$

where $\phi_{j,k} \approx \phi(x_j, y_k)$ are the point values, which are evaluated as follows.

We set $\phi_{j,k} = \phi_{\max}$ in the obstacle cells, while in the mixed and interior cells, we obtain $\phi_{j,k}$ by solving the Eikonal equations (3), (4) using the fast sweeping method from [17]. Note that the required pedestrian densities are computed from (5) in the interior cells and from the interpolation described in Sect. 2.1 in the mixed cells.

2.3 One-Sided Local Speeds of Propagation

In order to estimate the one-sided local speeds of propagation $a^{\pm}_{J+\frac{1}{2},k}$ and $b^{\pm}_{j,k+\frac{1}{2}}$ needed in (6) and (7), respectively, we first substitute (2)–(4) into Eq. (1) and rewrite it in the following nonconservative form:

$$\rho_t + \left[(u_{\max} - 2u)u\phi_x\right]\rho_x + \left[(u_{\max} - 2u)u\phi_y\right]\rho_y = \rho u \nabla\left(\frac{\nabla\phi}{\|\nabla\phi\|}\right), \tag{10}$$

and then locally freeze $\nabla\phi$. The one-sided local speeds then will be determined by the coefficients of ρ_x and ρ_y in the convective terms on the left-hand side of (10), which results in

$$a^{+}_{J+\frac{1}{2},k} = \max\left\{(u_{\max} - 2u^{\mathrm{E}}_{j,k})u^{\mathrm{E}}_{j,k}(\phi_x)_{J+\frac{1}{2},k}, (u_{\max} - 2u^{\mathrm{W}}_{j+1,k})u^{\mathrm{W}}_{j+1,k}(\phi_x)_{J+\frac{1}{2},k}, 0\right\},$$

$$a^{-}_{J+\frac{1}{2},k} = \min\left\{(u_{\max} - 2u^{\mathrm{E}}_{j,k})u^{\mathrm{E}}_{j,k}(\phi_x)_{J+\frac{1}{2},k}, (u_{\max} - 2u^{\mathrm{W}}_{j+1,k})u^{\mathrm{W}}_{j+1,k}(\phi_x)_{J+\frac{1}{2},k}, 0\right\},$$

$$b^{+}_{j,k+\frac{1}{2}} = \max\left\{(u_{\max} - 2u^{\mathrm{N}}_{j,k})u^{\mathrm{N}}_{j,k}(\phi_y)_{j,k+\frac{1}{2}}, (u_{\max} - 2u^{\mathrm{S}}_{j,k+1})u^{\mathrm{S}}_{j,k+1}(\phi_y)_{j,k+\frac{1}{2}}, 0\right\},$$

$$b^{-}_{j,k+\frac{1}{2}} = \min\left\{(u_{\max} - 2u^{\mathrm{N}}_{j,k})u^{\mathrm{N}}_{j,k}(\phi_y)_{j,k+\frac{1}{2}}, (u_{\max} - 2u^{\mathrm{S}}_{j,k+1})u^{\mathrm{S}}_{j,k+1}(\phi_y)_{j,k+\frac{1}{2}}, 0\right\},$$

where $u^{\mathrm{E}}_{j,k} = u_{\max}(1 - \rho^{\mathrm{E}}_{j,k}/\rho_{\max})$ and $u^{\mathrm{W}}_{j+1,k}$, $u^{\mathrm{N}}_{j,k}$ and $u^{\mathrm{S}}_{j,k+1}$ are obtain similarly.

3 Numerical Examples

We now test the proposed numerical method on a number of numerical examples. In all of the numerical examples below, the computational domain is $[0, 100] \times [0, 50]$. The upper and lower boundaries are solid walls, the exit is on the right (its size varies in different examples). In Examples 1, 3 and 4, the initial density is $\rho(x, y, 0) \equiv 0$ and the pedestrians enter the domain from the left, while in Example 2 the initial density is not zero and the left boundary is a solid wall. In all of the examples, the domain contains obstacles (as specified below) and we set $u_{\max} = 2$ and $\rho_{\max} = 10$.

Along the solid wall boundaries with no exits, we add one layer of obstacle cells, in which we set $\phi = \phi_{\max}$. In order to properly handle the exit on the right, we add two layers of cells on the right side of the computational domain. In the first additional layer, we place obstacle cells in those cells, whose entire left boundary coincides with the solid wall part of the original right boundary, interior cells in those cells, whose entire left boundary coincides with the open exit part of the original right boundary, and mixed cells otherwise. The second additional layer consists of interior cells. After the domain is extended, the shifted right boundary is set to be completely open, at which ρ is extrapolated from the left and ϕ is set to be zero.

At the inflow boundary (in Examples 1, 3 and 4), we obtain ϕ using the linear extrapolation from the right and set the following boundary condition for the numerical flux:

$$H^x_{\frac{1}{2},k} = \begin{cases} t/12, & 0 \le t \le 60, \\ 10 - t/12, & 60 \le t \le 120, \\ 0, & t \ge 120. \end{cases}$$

In Examples 1, 3 and 4, we use a 128×64 uniform grid, while in Example 2 we perform the experimental mesh refinement study. We note that a quite coarse mesh is used on purpose: our goal is to demonstrate that even though the proposed method is only first-order accurate near the obstacle, it is very robust and at the same time sharp at the discontinuities, which is important in practical applications, in which the use of a very fine mesh may be computationally unaffordable.

In Examples 3 and 4, we also compare the performance of our method with a naive method, in which all mixed cells are replaced with the obstacle cells, which is equivalent to extending the obstacle so that its boundary coincides with the cell boundaries. Our numerical experiments (not reported here for the sake of brevity) indicate that when the distance between the obstacles is sufficiently large, the latter approach leads to satisfactory results, which is not the case in Examples 3 and 4.

Example 1 We first consider the example studied in [16]. We take the solid obstacle to be the disk of radius 10 centered at (50, 20) and the exit is on the right between $y = 10$ and $y = 40$. In Fig. 1, we show a sequence of snapshots of the pedestrian density at times $t = 30$, 60, 120 and 180. The obtained results are in quite good agreement with the results reported in [16], but the shocks at time $t = 120$ are

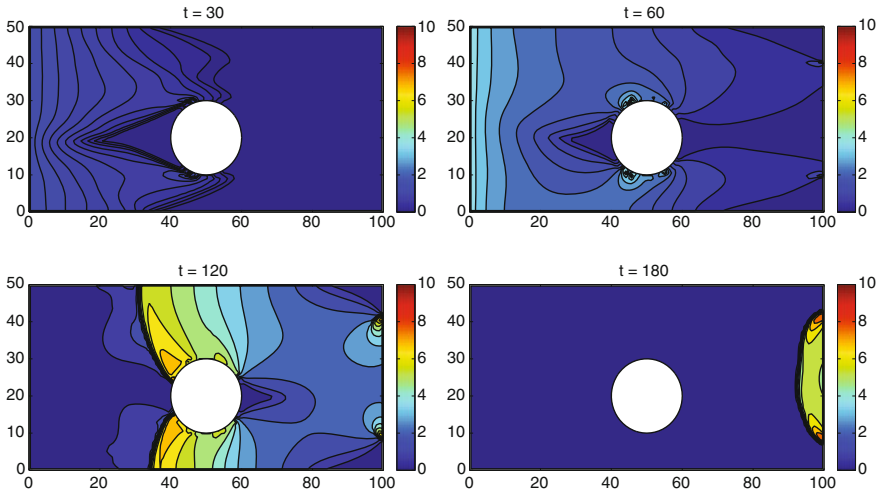

Fig. 1 Example 1: Density computed by the proposed method

Table 1 Example 2: Conservation errors in the cases of square and circular obstacles

Square obstacle			Circular obstacle		
Grid	Error	Rate	Grid	Error	Rate
128 × 64	3.77e-02	–	128 × 64	2.37e-02	–
256 × 128	1.95e-02	0.95	256 × 128	6.31e-03	1.91
512 × 256	1.02e-02	0.94	512 × 256	1.94e-03	1.70
1024 × 512	5.33e-03	0.93	1024 × 512	8.29e-03	−2.10

slightly sharper resolved by the proposed method and the solution at time $t = 180$ is not as smeared as the solution in [16, Fig. 4].

Example 2 In this example, we study the conservation error of our method. The initial density is

$$\rho(x, y, 0) = \begin{cases} 4, & x < 25, \\ 0, & \text{otherwise}, \end{cases}$$

and the exit on the right is the same as in Example 1.

We first take a 20 by 20 square obstacle centered at (50, 20) and compute the solution until the final time $t = 30$ by which the pedestrians reach the obstacle and start getting around it, but no one has left the domain yet. We compute the total density in the interior cells (where the density is evolved) and measure the relative conservation error on a sequence of uniform grids. The obtained results are reported in Table 1, where one can clearly observe that the expected first order of convergence has been experimentally achieved.

We then take the same circular obstacle, which was used in Example 1 and perform the same computations as in the case of the square obstacle. The conservation error behaves somewhat chaotic but remains bounded and within 1%.

Example 3 This is a modification of Example 1: the obstacle is shifted down by 8.5 so that the lower passage gets very narrow, which is a problematic situation for the naive method, which extends the obstacle and thus almost blocks the lower passage. We plot, in Fig. 2, the snapshots of the pedestrian densities at times $t = 30$, 60, 90, 120, 150 and 180, computed by both the proposed and naive methods. As one can see, the proposed method is capable of easily handling the narrow lower passage, in which the pedestrians get stuck for much longer time in the naive computation. In the latter case, we also observe a substantial delay in the pedestrian propagation in the area above the obstacle (see the results at time $t = 120$ and especially $t = 150$), which is attributed to the fact that more pedestrians are trying to move that way as the lower passage is almost blocked.

Example 4 In the final example, we make two substantial modifications to the data from Example 1. First, we take a larger circular obstacle of radius 15 centered at

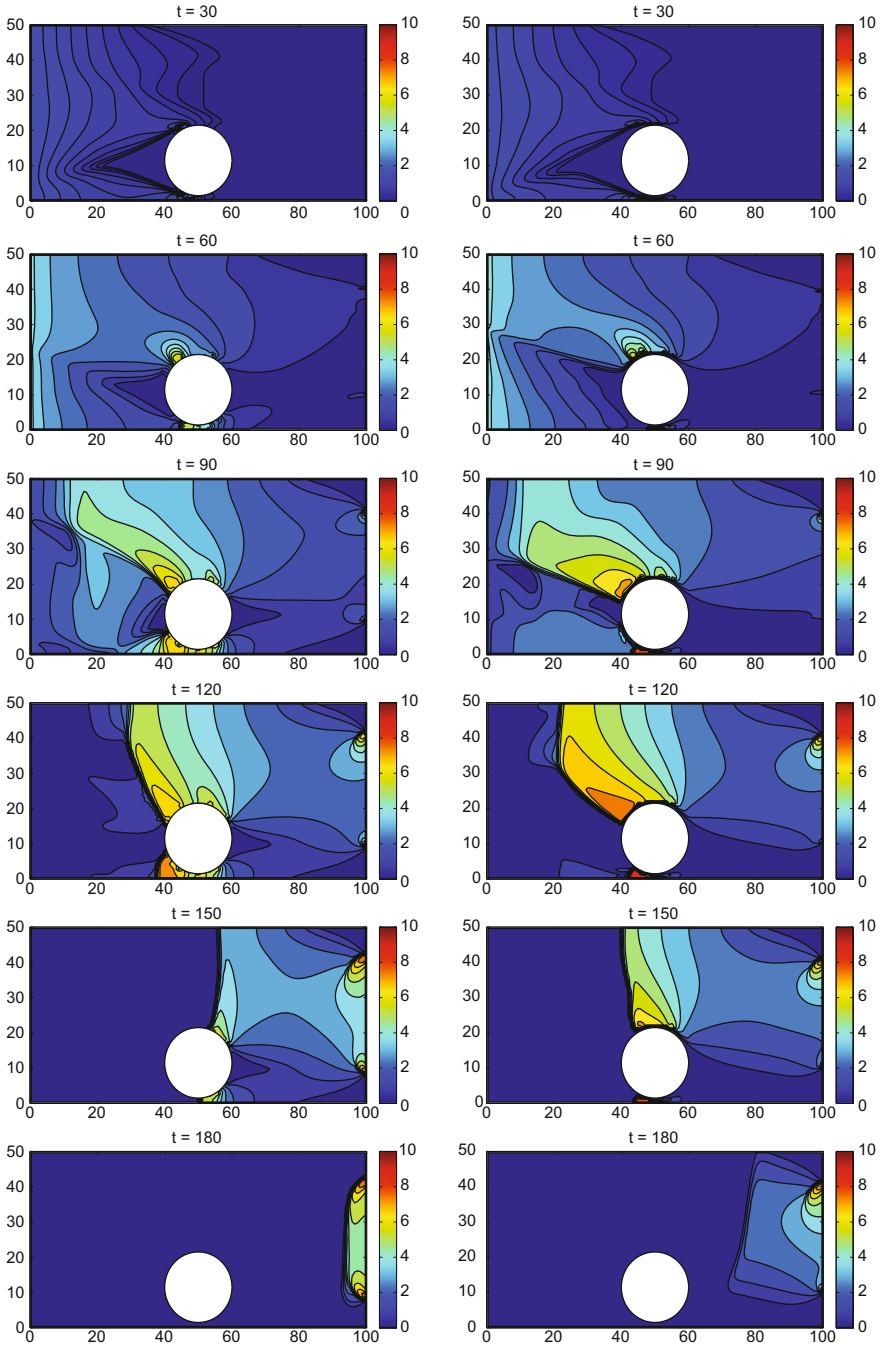

Fig. 2 Example 3: Density computed by the new (*left column*) and naive (*right column*) methods

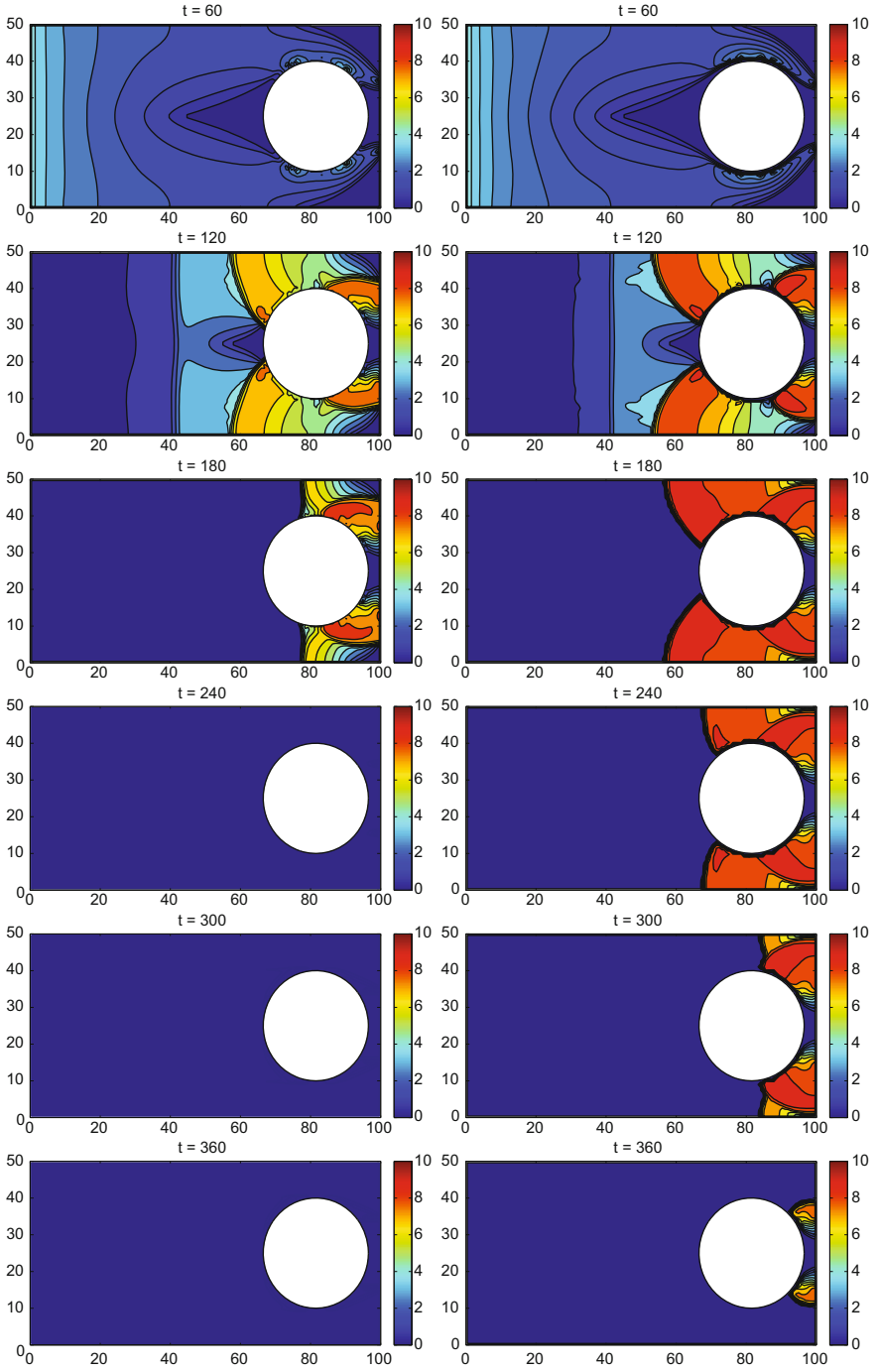

Fig. 3 Example 4: Density computed by the new (*left column*) and naive (*right column*) methods

(81.5, 25). Second, we take a more narrow exit on the right being now between $y = 15$ and $y = 35$. This makes the pedestrians to get substantially blocked when the obstacle is extended by the naive method; see Fig. 3 (right column), where a sequence of the density snapshots at times $t = 60$, 120, 180, 240, 300 and 360 is plotted. At the same time, the proposed method allows the pedestrians to pass through the narrow exit area without getting artificially stuck there; see Fig. 3 (left column). As one can see, when the proposed method is used, the pedestrian leave the domain by time $t = 240$, while in the naive computations they stay in the domain for much longer.

Acknowledgements The work of Y. Cheng and A. Kurganov was supported in part by the NSF grant DMS-1521009. The work of A. Chertock was supported in part by the NSF grant DMS-1521051.

References

1. Bollermann, A., Noelle, S., Lukáčová-Medvid'ová, M.: Finite volume evolution Galerkin methods for the shallow water equations with dry beds. Commun. Comput. Phys. **10**(2), 371–404 (2011)
2. Chertock, A., Epshteyn, Y., Hu, H., Kurganov, A.: High-order positivity-preserving hybrid finite-volume-finite-difference methods for chemotaxis systems (Submitted)
3. Chertock, A., Karni, S., Kurganov, A.: Interface tracking method for compressible multifluids. M2AN Math. Model. Numer. Anal. **42**, 991–1019 (2008)
4. Chertock, A., Kurganov, A.: A simple Eulerian finite-volume method for compressible fluids in domains with moving boundaries. Commun. Math. Sci. **6**, 531–556 (2008)
5. Gottlieb, S., Shu, C.W., Tadmor, E.: Strong stability-preserving high-order time discretization methods. SIAM Rev. **43**, 89–112 (2001)
6. Gottlieb, S., Ketcheson, D., Shu, C.W.: Strong Stability Preserving Runge-Kutta and Multistep Time Discretizations. World Scientific Publishing Co. Pte. Ltd., Hackensack (2011)
7. Huang, L., Wong, S., Zhang, M., Shu, C.W., Lam, W.: Revisiting Hughes' dynamic continuum model for pedestrian flow and the development of an efficient solution algorithm. Transp. Res. Part B **43**, 127–141 (2009)
8. Hughes, R.L.: A continuum theory for the flow of pedestrians. Transp. Res. Part B **36**, 507–535 (2002)
9. Kurganov, A., Tadmor, E.: New high resolution central schemes for nonlinear conservation laws and convection-diffusion equations. J. Comput. Phys. **160**, 241–282 (2000)
10. Kurganov, A., Tadmor, E.: Solution of two-dimensional riemann problems for gas dynamics without Riemann problem solvers. Numer. Methods Partial Differ. Equ. **18**, 584–608 (2002)
11. Kurganov, A., Lin, C.T.: On the reduction of numerical dissipation in central-upwind schemes. Commun. Comput. Phys. **2**, 141–163 (2007)
12. Kurganov, A., Noelle, S., Petrova, G.: Semi-discrete central-upwind scheme for hyperbolic conservation laws and Hamilton-Jacobi equations. SIAM J. Sci. Comput. **23**, 707–740 (2001)
13. Lie, K.A., Noelle, S.: On the artificial compression method for second-order nonoscillatory central difference schemes for systems of conservation laws. SIAM J. Sci. Comput. **24**(4), 1157–1174 (2003)
14. Nessyahu, H., Tadmor, E.: Non-oscillatory central differencing for hyperbolic conservation laws. J. Comput. Phys. **87**(2), 408–463 (1990)
15. Sweby, P.: High resolution schemes using flux limiters for hyperbolic conservation laws. SIAM J. Numer. Anal. **21**(5), 995–1011 (1984)

16. Xia, Y., Wong, S., Zhang, M., Shu, C.W., Lam, W.: An efficient discontinuous Galerkin method on triangular meshes for a pedestrian flow model. Int. J. Numer. Methods Eng. **76**(3), 337–350 (2008)
17. Zhao, H.: A fast sweeping method for Eikonal equations. Math. Comput. **74**(250), 603–627 (2005)